# Ultrashort laser - matter interaction at moderate intensities: two-temperature relaxation, foaming of stretched melt, and freezing of evolving nanostructures

Nail A. Inogamov[a], Vasily V. Zhakhovsky[b,c], Yurii V. Petrov[a], Viktor A. Khokhlov[a], Sergey I. Ashitkov[b], Kirill P. Migdal[d], Denis K. Ilnitsky[d], Yusuf N. Emirov[e], Konstantin V. Khishchenko[b], Pavel S. Komarov[b], Vadim V. Shepelev[f], Mikhail B. Agranat[b], Sergey I. Anisimov[a], Ivan I. Oleynik[c], and Vladimir E. Fortov[b]

[a]L. D. Landau Institute for Theoretical Physics, Russian Academy of Sciences, Chernogolovka 142432, Moscow region, Russia;
[b]Joint Institute for High Temperatures, Russian Academy of Sciences, Moscow 125412, Russia;
[c]Department of Physics, University of South Florida, Tampa FL 33620, USA;
[d]All-Russia Research Institute of Automatics, Rosatom, Moscow 127055, Russia;
[e]Advance Materials Research Institute, Florida Intern. University, Miami FL 33174, USA;
[f]Institute for Computer Aided Design, Russian Academy of Sciences, Moscow 123056, Russia

## ABSTRACT

Interaction of ultrashort laser pulse with metals is considered. Ultrafast heating in our range of absorbed fluences $F_{abs} > 10$ mJ/cm$^2$ transfers matter into two-temperature (2T) state and induces expressed thermomechanical response. To analyze our case, where 2T, thermomechanical, and multidimensional (formation of surface structures) effects are significant, we use density functional theory (DFT), solutions of kinetic equations in $\tau$-approximation, 2T-hydrodynamics, and molecular dynamics simulations. We have studied transition from light absorption in a skin layer to 2T state, and from 2T stage to hydrodynamical motions. We describe (i) formation of very peculiar (superelasticity) acoustic wave irradiated from the laser heated surface layer and (ii) rich complex of surface phenomena including fast melting, nucleation of seed bubbles in hydrodynamically stretched fluid, evolution of vapor-liquid mixture into very spatially extended foam, mechanical breaking of liquid membranes in foam (foam disintegration), strong surface tension oscillations driven by breaking of membranes, non-equilibrium freezing of overcooled molten metals, transition to nano-domain solid, and formation of surface nanostructures.

**Keywords:** Ultrashort laser pulse, two-temperature state, superelasticity, surface nanostructures

## 1. INTRODUCTION

We consider processes initiated by irradiation of metals by ultrashort laser pulse. Ultrashort means that duration of pulse $\tau_L$ is in the range from few femtoseconds (fs) to few picoseconds (ps). Optical radiation oscillates with periods $\sim 1$ fs. If duration $\tau_L$ is less than electron-ion temperature equilibration (eq) time $t_{eq} \sim 2-7$ ps then absorption of laser energy by electrons causes transition of metal into strongly pronounced two-temperature (2T) state[1] in our range of absorbed fluences $F_{abs} > 10$ mJ/cm$^2$, see Section 3 below. In the pronounced 2T state, the electron temperatures $T_e$ are 1-2 orders of magnitude above ion temperatures $T_i$. Duration of equilibration $t_{eq}$ is less than hydrodynamic time scale $t_s = d_T/c_s \sim 15-30$ ps depending on particular metal, here $d_T \sim 50-150$ nm is thickness of a heated surface layer created during 2T stage, $c_s \sim 3-6$ km/s is speed of sound. Heating at time scale $\tau_L$ less than $t_s$ induces expressed thermomechanical response.[2]

We emphasize that heating is fast, and that namely this rapidity links thermal and mechanical phenomena. In case of slow heating, the hydrodynamics is much less pronounced. In the case $\tau_L < t_{eq} < t_s$ considered here the thermomechanics is complicated by the 2T stage. In the case $t_{eq} < \tau_L < t_s$ the 2T effects are of

Further author information: (Send correspondence to N.A.I.)
N.A.I.: E-mail: nailinogamov@gmail.com, Telephone/fax: +7 495 702 9317

Fundamentals of Laser-Assisted Micro- and Nanotechnologies 2013, edited by Vadim P. Veiko, Tigran A. Vartanyan,
Proc. of SPIE Vol. 9065, 906502 · © 2013 SPIE · CCC code: 0277-786X/13/$18 · doi: 10.1117/12.2053166

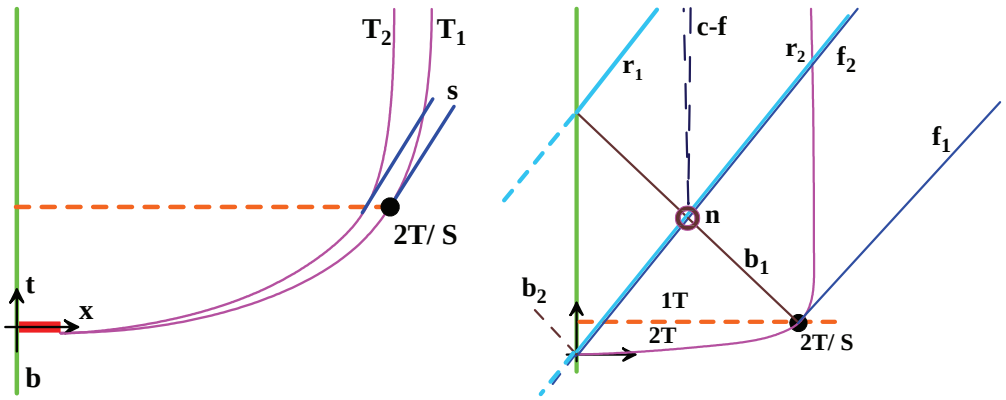


Figure 1. *Left panel.* Absorption of laser energy by electrons inside the red rectangular $\delta_{skin} \times \tau_L$ and fast propagation of absorbed heat into the bulk of target $x > 0$ (the magenta curves). The target boundary is shown as a green curve "b". Energy is transported by conduction band electrons (electron Fermi velocities $v_F$ are much higher than speed of sound $c_s$). At the 2T stage the diffusion of hot electrons is supersonic, therefore the tangential straight lines to the thermal wave trajectories (the magenta isothermal curves $T_1, T_2, ...$) are steeper than the trajectories of sound waves "s". Electron heat wave velocity sharply drops down below the speed $c_s$ at the transition from 2T stage to one-temperature (1T) stage. The orange dashed straight separates 2T and 1T stages. During the transonic transition around the label "2T/S" ($x = d_T, t = t_{eq}$) the acoustic wave detaches from the heat wave. The flux of acoustic characteristics is shown by the straight lines "s". *Right panel.* Three acoustic fluxes: forward $f_1 - f_2$, backward $b_1 - b_2$, and reflected flux $r_1 - r_2$. Imaginary images of b and r fluxes are shown as the dashed straight lines at the left side from the target boundary. Slightly above ablation threshold $F_{abl}$ the nucleation starts in the point "n" where the backward and reflected acoustic fluxes intersect. Above threshold $F_{abl}$, the cavitation zone "c-f" splits spallation plate from the remnant of a target. The spallation plate is the layer between the free boundary b and the left edge of the zone "c-f".

small significance, and the thermomechanical response may be described in the one-temperature $T_e = T_i = T$ approximation. To analyze our case with combined 2T and thermomechanical effects, we developed full 2T theory including 2T-equation-of-state (2T-EOS),[3] thermal transport properties of metals in 2T state,[3–7] and calculations of electron-ion coupling parameter[6,8–10] for simple metals,[8] for dielectrics,[9,10] and for noble and transition metals[6] where a situation is complicated by d-band influence; see also works.[11–15] This allows us qualitatively describe transition from light absorption to 2T state, and from 2T stage to hydrodynamics.

Hydrodynamics is split into two large sets of phenomena. From the one side this is formation of acoustic wave separating from the heated layer $d_T$ and propagating into bulk from irradiated frontal boundary (Sections 2 and 4). While from the other side, reflection of acoustic wave from frontal boundary with vacuum causes stretching of metal. If an amplitude of stretching is enough (critical amplitude) then nucleation in molten metal layer begins (Sections 2 and 5). Calculations show that for all considered metals critical amplitude is achieved significantly above a melting threshold. Therefore rupture of continuous matter connected with nucleation begins in liquid.

The both sets of phenomena are considered in details (Sections 4 and 5). It is shown that a separation of acoustic wave from the layer $d_T$ is accompanied with formation of kink in a stress profile, and that elastic-plastic transformations take place at unusually high stresses (superelasticity). The kink is a trace of a fast (supersonic) melting phase transition called also homogeneous melting.

It is proved that the nanosecond time scale surface tension oscillations and fast non-equilibrium freezing of overcooled liquid metals are the key ingredients in the process of nanostructures formation after single or limited number shots irradiation of metals with initially well polished surface (Section 5).

## 2. GENERAL PICTURE

Processes initiated by ultrafast irradiation cover wide spatiotemporal range beginning from absorption during first femtoseconds and lasting till to nanoseconds when freezing finishes; while plume flies and evolves up to arrival to some remote collector. Let us consider pulse durations $\tau_L = 50 - 200$ fs used in our laser experiments

described in Section 5 below. A set of the processes form a hierarchy of different increasing orders in the spatiotemporal domain. This set is: [i] absorption {15 nm, 0.1 ps}, [ii] 2T stage {$\sim$ 100 nm, $\sim$ 1 ps}, [iii] one-temperature (1T) hydrodynamic stage begins {$\sim$ 100 nm, $\approx$ 20 ps}, [iv] total freezing finishes {$\sim$ 100 nm, $\sim$ 1000 ps = 1 ns} and hydrodynamic motion near surface stops; of course, in case of a thick target an acoustic wave continues its propagation into bulk. We show comparisons between the processes [i] and [ii] at a $x,t$-diagram in Fig. 1 (left), and between the processes [ii] and [iii] in Fig. 1 (right), While the processes [iii] and [iv] are compared in this Section a bit below.

As was said, the shortest $x,t$-scales are connected with absorption stage. They are skin layer thickness $\delta_{skin} = 10 - 20$ nm and pulse duration $\tau_L$. Region corresponding to absorption is presented by a red rectangular in Fig. 1 (left). Distance $x$ and time $t$ in Fig. 1 are reckoned from the initial position of boundary b in Fig. 1 and from the instant of arrival of maximum intensity of Gaussian in time laser pulse at the target boundary. Key spatial scale $d_T$ is linked to a heat propagation at a 2T stage. 2T scales $d_T$ and $t_{eq}$ are order of magnitude larger than the scales at an absorption stage. We are interested to study fluences of the order of and higher than an ablation threshold $F_{abl}$ J/cm$^2$ since around this threshold hydrodynamics becomes one of the dominant processes. This circumstance does the picture interesting.

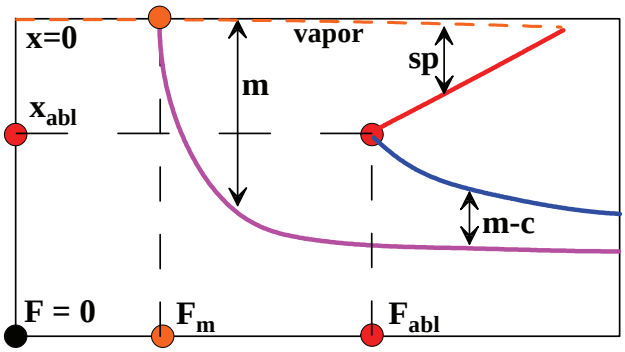


Figure 2. Absorbed fluence - depth diagram. Vertical axis shows Lagrangian depth $x_{Lagr}$ measured from initial position of vacuum boundary. The Lagrangian coordinate corresponds to initial position of material particle. Horizontal axis presents the absorbed fluence $F_{abs}$. Maximum molten depth $x_{Lagr}(F_{abs})$ is given by the magenta curve "m". It starts from a boundary at a melting threshold $x_{Lagr}(F_{abs}|_m) = 0$. Spallation plate "sp" appears above an ablation threshold $F_{abs}|_{abl}$. The plate exists in the finite range of fluences $F_{abs}|_{abl} < F_{abs} < F_{abs}|_{ev}$, where $F_{abs}|_{ev}$ is evaporation threshold.[4,16–20] Let us emphasize that there are a layer of evaporated mass marked by the dashed curve "vapor". Up to ablation threshold, a mass thickness of this layer of pure vapor is small in comparison with depth $x_{abl}$.

Simulations show that in metals the value $F_{abl}$ is 2-3 times above the melting threshold $F_m$, see Fig. 2. Since ablation threshold $F_{abl}$ is significantly higher than melting threshold $F_m$, then the overheating above a melting curve during 2T relaxation is large for fluences $F \sim F_{abl}$ and higher. Therefore metal melts fast at the relatively short 2T stage, and supersonic melting follows supersonic heat penetration for those fluences. Such melting is also called homogeneous or volume melting. Let us mention that the threshold $F_m$ is not very well defined quantity since there is finite width two-phase transition zone where a solid and liquid coexists in form of a mixture. This circumstance defines smearing of the threshold $F_m$.

Transition from supersonic heat propagation at the 2T stage to 1T hydrodynamics separates thermal and mechanical stages. Thermal layer $d_T$ remains near surface and slowly cools down* as result of heat loses into cold bulk (see Fig. 3 right), while acoustic wave detaches from the layer $d_T$ and runs into the bulk. Acoustic wave propagating into the bulk is formed from forward "f" and reflected "r" fluxes of characteristics, see Figs. 1 and 3. The f-flux carries positive pressure values and forms compression part of the propagating wave. The r-flux appears as result of reflection from vacuum boundary. This reflection reverses a sign of pressure, therefore the r-characteristics carry negative values of pressure. They form tensile part of the propagating wave.[21–24] When fluence $F_{abs} < F_{abs}|_{abl}$ is small, then positive and negative amplitudes are approximately equal. For the higher values of $F$ the absolute value of negative pressure in the wave is significantly below the positive value $p_+$, even for values of $p_+$ which are significantly less than a bulk modulus $K$. This is so because a strength of matter $\sigma_{res}$ to resist to stretching is significantly less than a bulk modulus $K$. Value of the maximum absolute value of negative pressure $p_{cold}|_{max}$ at a cold curve is a measure of nonlinearity for stretching, rather than a modulus $K$, since value $p_{cold}|_{max}$ is few times less than the modulus $K$. At the same time, a strength $\sigma_{res}$ of metal in our experimental conditions with ultrahigh deformation rates $\dot{V}/V \sim 10^9$ s$^{-1}$ is higher than a strength at moderate

*Of course, the process of conductive cooling depends on thickness of a target. Thin films $d_{film} < d_T$ do not cool down to room temperature (this is initial temperature in our experiments), since they do not have thermal sink.

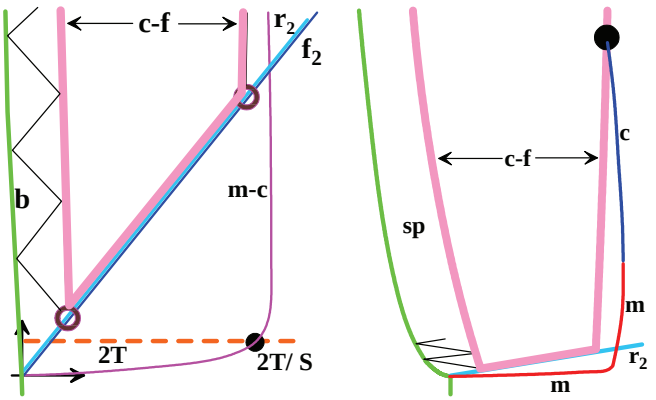


Figure 3. Foam formation and expansion. Foam appears when fluence is significantly above threshold $F_{abl}$. *Left panel.* Above threshold $F_{abl}$, nucleation of nanovoids continues at a finite interval along the characteristics $r_2$. This is the interval between two empty circles. The characteristics $r_2$ is a head of a reflected wave where stretching has maximum. The interval becomes wider when fluence is larger. Length of the interval tends to zero in the limit $F \to F_{abl}$ when $F$ decreases, see Fig. 1 (right). Molecular dynamics (MD) shows that appearance of new voids along the interval is not homogeneous, there are flashes of nucleations. Number of flashes increases as value $F/F_{abl}$ increases. *Right panel.* Late stage of foam evolution, its disintegration, and freezing near the foam-target contact. Below ablation threshold $F_{abl}$ the shift of the free (fr) boundary (the left green curve) $\int_0^t v_{fr}(t')dt'$ exhibits (i) ultrashort powerful acceleration lasting few atomic time scales (subpicosecond; for pulse durations less than Debye inverse frequency); this is an acceleration under action of pressure of excited electrons; (ii) deceleration connected with resistance of continues matter to stretching; this deceleration acts during acoustic time scale $t_s = d_T/c_s$; (iii) smooth transition to the rest state where the boundary stops: $v_{fr} \to 0$, when the b-characteristics around the characteristics $b_1$ (see Fig. 1, right) arrive at the boundary. Above the threshold $F_{abl}$ the shift $\int_0^t v_{fr}(t')dt'$ exhibits (i) powerful acceleration; (ii) deceleration-1 due to resistance of continues matter; this deceleration lasts up to arrival of the left nucleation shock at the free boundary; (iii) deceleration-2 as result of resistance of foam to its stretching; value of deceleration by foam is less than the value of deceleration by continuous molten metal; nevertheless this deceleration is dynamically important; at the stage (iv) average in time deceleration becomes zero, spallation plate flies with fixed average velocity $v_{fr}(t = \infty) > 0$. The c-f (cavitation-foaming) gap is not empty, it is filled with two-phase vapor-liquid mixture. The mixture evolves from small content of vapor bubbles to foam with small liquid content. Late in time foam decays into cloud of droplets in vapor surrounding. We will see below in Section 5 devoted to MD simulation that disintegration of foam near the right edge of the gap kinematically is a slow processes. Therefore solidification may freeze the remnants of the foam disintegration before they will be smoothed out by surface tension. Crystallization front is marked "c". Solidification finishes when the front "c" arrives at the right edge of the gap "c-f" with foam. The instant of arrival is distinguished by the black circle.

and low rates $\dot{V}/V$ .[25–27] Our values of experimental and computed strength $\sigma_{res}$ tend to an atomistic strength, defined by quantum interatomic interactions: $\sigma_{res} \sim p_{cold}|_{max}$.

The wave formed from f- and r-characteristics (f,r-wave) is nonlinear. Ratio of its maximum amplitude of pressure to bulk modulus $(p+)/K$ is $\sim 0.2$ at an ablation threshold $F_{abl}$. This ratio increases with absorbed fluence. Outside the thermal layer $d_T$, this is a Riemann plane simple wave propagating in homogeneous medium. The f,r-wave is composed from forward, middle, and back pieces. The forward piece is formed from f-characteristics. Transition between f- and r-fluxes is the middle piece. While the r-flux is the back piece, see Fig. 1 (right). At an early hydrodynamical stage $t \sim t_s$, forward and back pieces have sloping profiles with moderate gradients, and their lengths are of the order of $d_T$. While the middle piece is short and steep, see pictures in papers.[9,18,21,28] That is, the early profiles replicate the temperature profile shifted along the propagation axis $x$. They are far from profiles with shocks. The forward piece is a direct replication of temperature profile, and the back piece is an reversed back replication. Namely this reversal near the characteristics $f_2, r_2$ starting from a free boundary is responsible for the steep middle piece of the running f,r-wave.

As result of nonlinearity the f- and r-characteristics are not parallel to each other since they carry different values of pressure. These characteristics focus at the forward and back pieces of the wave, and defocus at the middle piece. Therefore the sloping pieces become steeper, while the steep middle piece becomes more

sloping.[9,18,21,28] Focusing and steeping of the forward piece leads to breaking (overturning) of the wave and to formation of shock in the point of inflection. Later an amplitude of the jump increases, and shock wave with triangular shape appears. This shape is obviously opposite to the early profiles replicating spatial temperature distribution. The process of nonlinear evolution of wave is described in papers.[23,29–33] The description in those papers is based on molecular dynamics (MD) simulations. Below in Section 4 we presents new results concerning comparison the 2T-hydrodynamic simulations † and MD.

Nucleation slightly above an ablation threshold $F_{abl}$ creates slowly expanding cavitation zone, see Fig. 1 (right). Below threshold $F_{abl}$ the characteristics $b_1$ propagates to the left side up to the free surface. It reflects from the free surface as reflected characteristics $r_1$, see Fig. 1 (right). Thus the back piece of the f,r-wave is formed below $F_{abl}$. If $F > F_{abl}$ then the situation changes qualitatively - above the nucleation point the characteristics $b_1$ passes away. Nucleation shocks appears instead of the characteristics $b_1$ and $r_2$. There are two nucleation shocks - one propagates to the left side, while the other propagates to the right. The back piece of the f,r-wave disappears as whole in the situation $F > F_{abl}$.

At the same time the forward piece of the f,r-wave survives after nucleation because it travels ahead relative to the right nucleation shock. Evolution of the forward piece is independent relative to the nucleation event up to the instant of formation of triangular shock wave. In this shock the maximum of pressure is achieved exactly after shock. The overturning of the profile and formation of shock in the point of inflection take place along the flux of the f-characteristics running to the right side with speed of sound. Therefore this phenomenon is not influenced by cavitation behind it. The f-flux gradually disappears in the growing right shock. The last f-characteristics is the characteristics $f_2$. It carries maximum pressure $p+$. The characteristics $f_2$ vanishes in the shock in the instant $t_m$ when the shock achieves the maximum $p+$. Before the instant $t_m$ the pressure along the instant pressure profile grows from right to left - from the value behind shock to the value $p_+$. After this instant the pressure behind the shock front begins to decrease as result of rarefaction. The picture of shock formation (as result of overturning) and evolution of elastic and plastic shocks shown in the eighth figure in paper[33] are applicable here. Although the simulations carried in paper[33] correspond to the case when a thick glass window supports the irradiated metal boundary and there is no cavitation as in our case with mechanically free irradiated frontal boundary.

The left and right nucleation shocks come as result of interference of many shocks around individual nanovoids expanding at an early stage after their appearance with velocities of the order of sound velocity. The left nucleation shock oscillates inside the spallation plate as shown in Fig. 3. Those multiple reflections of the left shock cause velocity oscillations $v_{fr}(t)$ of the shifting $\int_0^t v_{fr}(t')dt'$ free (fr) boundary.[23,29,31] This phenomenon is well known from physics of shocks.[34–37] Usually it is observed in the orders of magnitude larger spatial scales. It is interesting, that below ablation threshold $F_{abl}$ focusing of characteristics leads to not only overturning of the forward piece of the f,r-wave described above, but the focusing of the r-characteristics leads to overturning and formation of shock in the back piece of the f,r-wave. The r-characteristics focus since the r-characteristics more close to a free surface carry larger values of pressure than the r-characteristics ahead them. The r-shock is a jump of pressure from negative value to a zero value. It presents continuation of a Hugoniot adiabat into the region of negative pressures of rather large amplitudes: from few to few tens GPa (it is different for different metals). The circumstance that those amplitudes are large, is a special feature of the ultrashort irradiation. Below the threshold $F_{abl}$, this negative shock replaces the right nucleation shock.

## 3. PROPERTIES OF METALS IN THE STATE WITH HOT ELECTRONS

Ultrashort laser pulse transfers metal into state with excited electron subsystem, since laser energy is absorbed by electrons in intraband and interband transitions and since there is a large difference in electron and ion masses; this difference slows energy exchange. Rate of thermalization of excited electrons and evolution of electron distribution function to Fermi distribution are defined by frequency of electron-electron collisions $\nu_{ee}$. This frequency has been calculated.[5,6] Rough estimate is $\nu_{ee} \approx (v_F/a)(k_B\,T_e/E_F)^2$, where $v_F$ is Fermi velocity, $a$ is interatomic spacing, $E_F$ is Fermi energy, $v_F/a \sim 1$ fs$^{-1}$; room temperature value is $\nu_{ee} \sim 10^{11}$ s$^{-1}$. Thus

†In the Section 4 the recently developed modification of 2T-hydrodynamical code is presented. For the first time it includes elasticity effects together with 2T-effects.

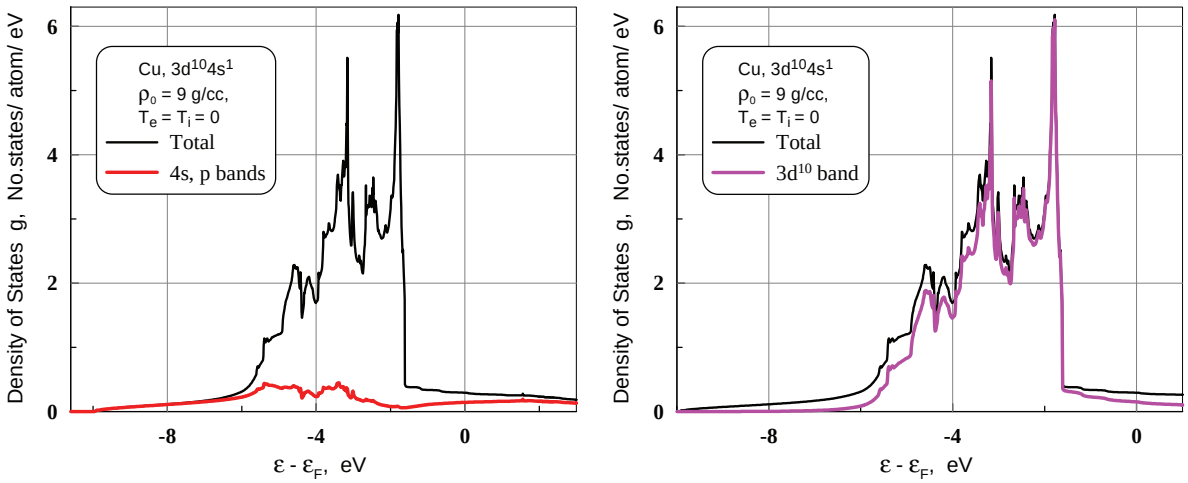


Figure 4. DOS of copper in normal conditions. *Left panel.* The left energy edge of allowed states is defined by 4s-band. The s-electrons also dominates above the upper edge of the d-band. Energy is given relative to Fermi level $\varepsilon_F$. This is a chemical potential at zero electron temperature: $\varepsilon_F = \mu(T_e = 0)$. *Right panel.* The d-band containing 10 electrons dominates in the energy zone occupied by d-electrons at $T_e = 0$. The tail of d-band above the sharp right edge appears due to hybridization and some inaccuracies of calculations.

thermalization time $t_{ee}$ decreases as electron energy increases. Estimates show that absorption of few mJ/cm$^2$ decreases time $t_{ee}$ down to duration of our laser pulse $\tau_L \sim 100$ fs. We are interested in cases with values $F_{abs}$ are of the order of few tens of mJ/cm$^2$. Therefore we can surely treat electrons as distributed according to Fermi function with current local temperature $T_e(x,t)$. The rate of thermalization of phonon degrees of freedom $t_{ii} \sim 0.1 - 1$ ps is of the order of inverse Debye frequency $1/\omega_D$. There are interesting problems concerning coherent phonon oscillations, Glauber states, and entangled phonons.[38,39] Coherent phonon oscillations may be excited by ultrashort laser pulse when duration is small $\tau_L \ll 1/\omega_D$ [38–40] We will not consider these questions here. Namely, following the paper,[1] we limit ourself to the case when electron and ion subsystems are described by their temperatures $T_e$ and $T_i$.

Excitation of electrons changes thermodynamics and EOS. We use DFT (Density Functional Theory) to define pressure and internal energy as it was done in the papers.[3,11,41,42] We separate electron and ion contributions according to paper.[3] Figs. 4 and 5 present new results concerning copper [Ar]3d$^{10}$ 4s$^1$. Electron spectra and cold curves for fcc Cu are shown. Simulations have been performed by VASP package.[43] Only valence band electrons are included. Internal electron shells are separated by wide energy gap. Their influence is taken into consideration by applying the PAW LDA pseudopotential. Parameters are: a plane-wave cutoff 500 eV, $21^3$ k-points, and 25 electron bands. Details of simulation will be presented elsewhere. Here it is necessary to give an outline of 2T model used for our hydrodynamic and MD calculations. Figs. 4 and 5 (left) show electron density of states for normal density, cold copper. Role of stretching and compression of fcc lattice (variation of $\rho$) together with analysis of influence of increasing of electron temperature $T_e$ will be given separately since volume of the paper is limited. Compression does spectrum wider, it separately deforms partial spectra of s- and d-band electrons. While the lose of d-band electrons due to heating of electron subsystem and excitation of d-electrons results in the shift of the d-band down along the energy axis and in the contraction of the d-band.

Figs. 4 and 5 (left) present total and partial electron spectra. Previously only total density of states (DOS) have been presented. Partial DOS describe 3d and 4s,p bands separately. This separation allows to clarify parameters used in two-parabolic approximation of electron spectrum. Calculations of transport coefficient and electron-ion energy exchange coefficient (coupling parameter)[5–7] are based on this approximation.

Fig. 5 (right) shows how cold pressure varies as result of isotropic 3D stretching and compression of the fcc lattice. The curve "Rose" is obtained according to analytical expression given in paper.[45] This expression includes anharmonicity effects and experimental data. It agrees well with Hugoniot data.

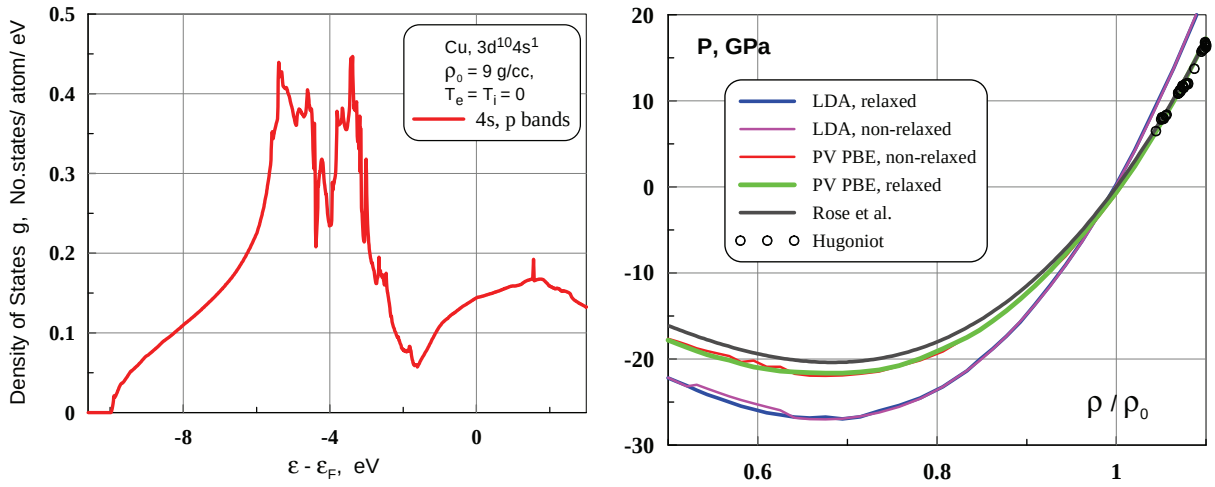


Figure 5. *Left panel.* The s-band. The scale for the g-axis is enlarged in comparison with Fig. 4. *Right panel.* Cold pressure and experimental Hugoniot adiabat taken from[44] are shown. Up to moderate compressions the thermal effects are small, and the dependence of cold pressure follows the Hugoniot adiabat. The curve "Rose" presents analytical dependence from.[45] The PV PBE calculations better agree with the Rose curve and Hugoniot than the LDA.

There are four atoms in a cubic cell in a fcc crystal. This cubic cell is used in DFT quantum calculations since this is a configuration containing minimal number of atoms, and since it allows easily satisfy the 3D periodic boundary conditions. The cubic cell has four primal unit cells. Every unit cell has only one atom per unit cell. The unit cell has a shape of an oblique parallelepiped. Fcc crystal has only acoustic modes of lattice oscillations, since there is only one atom per a unit cell. "Non-relaxed" calculations illustrated in Fig. 5 (right) correspond to the case with fixed positions of the four atoms in a cubic cell. While in the "relaxed" calculations it is allowed to shift[‡] slightly atoms from their exact lattice positions to achieve better convergence. The "relaxed" and "non-relaxed" curves agree well in Fig. 5 (right). This is a good sign, it means that there are no polymorphic transitions near the fcc configuration and that calculations are of good accuracy. Some small deviations appear in the range of ultimate stretching near the spinodal where crystal can decay due to a lattice instability. In the case of four atoms per cell and 3D periodic boundary conditions this may be decay of a fcc lattice into a set of separate parallel planes.

## 4. GENERATION OF SHOCK

It is well known that lasers are effective generators of shocks in condensed media. There are many papers concerning this application of lasers, but here we distinguish those of them where superelastic shocks have been observed. In a superelastic shock a crystal survives under unusually strong uniaxial compression, while the plastic transformations are absent or significantly delayed. Propagation of shocks initiated by subpicosecond pulse has been studied in works done by Evans et al.,[46] Gahagan, Moore, Funk et al.,[47,48] and Ashitkov, Agranat, Kanel' et al.[25–27,49] Existence of superelastic shocks have been found also in experiments with subnanosecond pulses done by Whitley et al.[50] and Crowhurst, Armstrong et al.[51] Those experimental results on the superelastic shocks have been explained and supported theoretically.[25,33,52–54]

There are two groups of experiments: they are subpicosecond[26,46,47] and subnanosecond[50,51] experiments. Spatial scales (thickness of used films) are of the order of micron[§] for both groups. In the first group there is unsupported superelastic shock propagating through the film (triangular elastic shock). In the second group the superelastic shock is continuously supported during its propagation (support by a laser drive, a rectangular elastic shock). Therefore superelasticity is not directly connected with the shortness of loading. Indeed, in the subpicosecond case a thickness (FWHM) of shock compressed elastic layer is 50-100 nm, and duration of existence

[‡]Though, as was said, an *ideal* lattice corresponding to $T_i = 0$ is considered.

[§]The largest thicknesses of an Al films are 10 microns in the sub-ps work[55] and 8 microns in the sub-ns work.[50]

of metal in the compressed superelastic state is 10-20 ps.[25,33,54] In the studied so far subnanosecond case[50,51] this thickness is orders of magnitude larger (few hundreds of nanometers). The papers[53] and[33,54,56] introduce new classification of the shock wave regimes. In the previous arrangement the 2W2Z¶ regime changes to the 1W1P‖ regime as an amplitude of a shock grows. The transition is in the point OD (overdriven) where, as was thought, the plastic shock overruns the elastic one since plastic becomes faster than elastic wave because propagation velocity of elastic (is thought) is limited by Hugoniot elastic limit (HEL). In the new arrangement the 2W2Z and 1W1P regimes are separated not by a point OD. There is an intermediate regime 1W2Z** between them. The regime 1W2Z covers a finite interval of pressure amplitudes $p_{pl}$ behind a plastic shock. In this interval the distance $d_{el-pl}(p_{pl})$ separating shocks decreases from an infinite value at $p_{pl}|_1$ to the value $d_{el-pl}(p_{pl}|_2) \sim a$ at pressure $p_{pl}|_2$ where $a$ is interatomic scale. Of course, an accurate definition of the value $p_{pl}|_1$, which splits up the 2W2Z and 1W2Z cases, is limited by accuracy of measurements and thickness of films. While the value $p_{pl}|_2$ is defined by the Rayleigh line and the value called HEL-star in papers.[33,53]

There are three important, qualitatively new phenomena linked with the laser shocks. They are: (i) the mentioned above superelasticity; (ii) formation of the two-zone (elastic and plastic) single shock waves (1W2Z),[53] see also;[33,54,56] and (iii) a complex interaction between homogeneous melting and formation of elastic-plastic shock during the process of separation of hydrodynamical wave from the supersonically created thermal layer $d_T$, see Section 2 and Fig. 1. It is found that changes in compressibility in the melting zone during heating along an isochoric thermodynamic trajectory deform the pressure profile, and it is found that this deformation is carried out by f-characteristics, therefore the deformation remains imprinted into the pressure profile of the hydrodynamical wave.[57,58] The imprint represents a more steep piece of profile where a gradient is enlarged. Value of pressure $p_{int}$ at this piece is defined by intersection of the isochoric line and the melting curve, and therefore this value does not depend on absorbed fluence. The steep piece provokes early overturning and formation of elastic shock[33] with amplitude of pressure defined by the value $p_{int}$. The amplitude of an elastic shock after its formation weakly depends on fluence $F_{abs}$. Here we present new results explaining the reasons why the steep piece of profile appears, see Figs. 6. We use modification of 2T-HD code where the hydrodynamics has been turned off: $u(x,t) \equiv 0$. This version describes 2T stage when a thermal wave propagates supersonically and we can neglect in the first order the motion in a narrow zone near the vacuum-metal boundary.

Formation and supersonic propagation of the steep piece DE of profile, in the case when 2T-effects and hydrodynamics both are taken into consideration (code 2T-HD), are shown in Fig. 7 (left). The piece DE appears after melting. Profiles for the three instants ($t = -40$ fs, 0.6 ps, and 1 ps) are shown. Time is reckoned from the instant of maximum power of a pump pulse $\tau_L = 100$ fs. The compressive part of the profile ABC for $t = -40$ fs is separated from the melting curve "melt". Therefore the steep piece is absent for this very early instant. Rarefaction tail BC of the three profiles ABC (-40, 600, and 1000 fs) shows interesting phenomenon of "cold evaporation" under action of electronic pressure $p_e$ stretching metal near boundary above a strength of metal. The dynamic boundary condition, hold at the vacuum-metal surface, says $p = 0$. Since $p = p_e + p_i$ this condition means that positive $p_e$ creates tensile stress stretching matter near boundary. In the points C, running relative to matter, metal intersects the strength curve "ef.sp", see Fig. 7 (left). This is an effective spinodal used as criterium for rupture in this 2T-HD simulation. It is adopted in the version of wide-range 2T-EOS used for this simulation.[3,34,44] The spinodal corresponding to the wide-range EOS[34] is the curve "spin" in Fig. 7 (left). Strength of aluminum "strn" according to EAM potential and to our deformation rates is also shown. It is taken from paper.[25] The teared off Lagrangian points form a tail scattered at the right side relative to the points C. The computer run shown in Fig. 7 (left) is made for the case $F_{abs} = 130$ mJ/cm$^2$. There are few atomic layers ablated thanks to mechanism of "cold evaporation". This amount is larger for larger fluences $F_{abs}$. Layers are

¶2 waves 2 zones. The first zone is an elastic zone, the plastic zone follows it (2Z). We say two-waves (2W) because the elastic and plastic shocks move with different velocities and splitting between them increases with time. This is obviously unsteady wave structure.

‖1 wave 1 zone - purely plastic shock with transition from an elastic state ahead the shock to a plastic state behind it in a thin layer with thickness of the order of few interatomic distances.

**1 wave (1W) two-zone (2Z, elastic and plastic) single wave structure. In this structure the acoustic irradiation from the plastic front supports the elastic shock. The irradiation does not allow to attenuate the elastic shock. This is a quasi-stationary structure with the constant in time averaged in time an intershock distance $d_{el-pl}(p_{pl})$. In the steady state shock the supporting pressure $p_{pl}$ is constant in time.

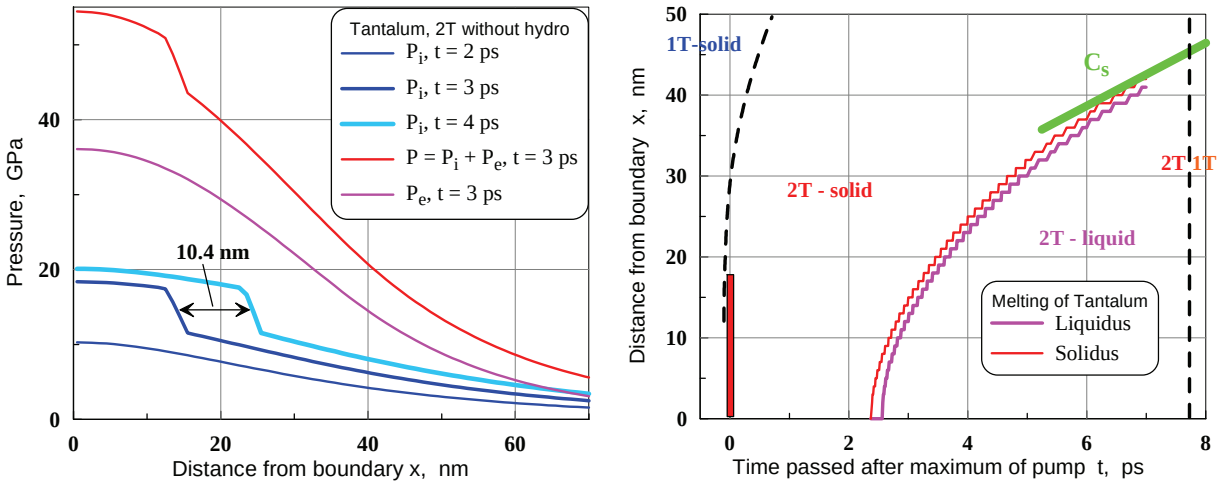


Figure 6. Tantalum, $F_{abs} = 0.2$ J/cm$^2$. *Left panel.* Evolution of pressure profiles in an isochoric regime when we can neglect hydro-motion. Pressures $p_e(\rho, T_e), p_i(\rho, T_i)$ ,[3] and $p = p_e + p_i$ follow temperature profiles $T_e, T_i$ defined by an expanding thermal wave. Thermal wave is supersonic therefore the changes of pressure are also supersonic: the shift marked by the two-head arrow has a Mach number 2.5. Melting and rise of Gruneisen parameter in a two-phase solid-mixing zone caused by phase transition lead to appearance of the steep piece. This piece is absent before melting, while after melting it is present only on the $p_i$ -profiles and on the profiles of total pressure. A profile of electron pressure $p_e$ remains smooth. *Right panel.* Supersonic (comp. slopes of melting front and acoustic straight $c_s$) melting called also homogeneous melting. Sides of the red rectangular are $\tau_L = 100$ fs and $\delta_{skin} = 15$ nm, see Fig. 1 (left). According to MD simulations the two-phase solid-liquid zone between solidus and liquidus is wider and less definite in comparison with the finite differences 2T simulation.[59] But instant positions of the melting zone trajectory agree. In such refractory metal as Ta, the electron-ion temperature equilibration lasts rather long time. Coupling parameter for Ta has been calculated in.[6] We stop the 2T calculations near the end of 2T relaxation since this code does not include motion. The straight $c_s$ (tangential to the melting front at the end of 2T stage) has a slope equal to speed of sound. The dashed curves "2T-1T" separates 2T and 1T stages. Outside of the 2T spatiotemporal region, the melting transits to the usual slow, subsonic regime of propagation and heterogeneous melting with a thin melting zone, see Figs. 1 and 3.

ablated layer after layer. This is different from spallation of a layer of finite thickness under action of electron pressure, considered in papers.[60–62] The "cold evaporation" has obvious threshold connected with finite strength to resist to stretching.

2T-HD code developed to describe combination of 2T-effects and hydrodynamics has been developed further to include elasticity (2T-HD+Elast code) since as was said above in laser experiments elasticity survives up to very large stresses. Here we present first results of this development, see Figs. 7 (middle and right). A longitudinal stress is $p_{xx} = p_i + p_e - s_{xx}$, where shear is $s_{xx} = (4/3)G\,(\partial x/\partial x_0 - 1)$, $G$ is shear modulus, and $x(x_0, t)$ is trajectory of Lagrangian particle $x_0$. The shear (absolute value) in our approach smoothly decreases in the transition layer from solid to molten phases, since we suppose that it is proportional to a volume fraction of solid in a solid-liquid mixture. In the 2T-HD+Elast code an aluminium is softer than in MD, see Figs. 7 (middle and right) therefore the Hugoniot adiabat corresponding to 2T-HD+Elast code locates between an elastic Hugoniot according to EAM used in MD and the plastic Hugoniot corresponding to the code 2T-HD.

## 5. FOAMING AND SOLIDIFICATION

As was shown in Section 2, hydrodynamic decay of a pressurized surface layer $d_T$ leads to formation of forward f- and backward b-wave, see Fig. 1 (right). The b-wave transfers into r-wave after reflection from boundary. In case of contacting media with large difference in acoustic impedances (here there is a vacuum-metal contact) the r-wave is a tensile wave stretching metal. The f- and r-waves leave a surface layer $d_T$ during acoustic time scale $t_s = d_T/c_s$. But interesting near-surface dynamics does not finish after departure of the f-, r-waves if a nucleation threshold $F_{nucl}$ is exceeded. New phenomena appear above a threshold $F_{nucl}$. Those phenomena

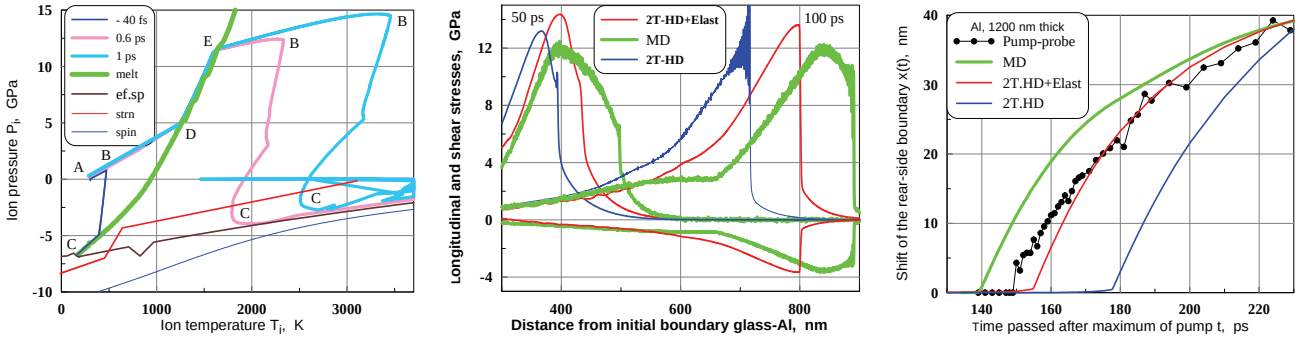


Figure 7. *Left panel.* Appearance of the steep piece DE as a result of fast melting in the case when hydrodynamics is included (Al, $F_{abs} = 130$ mJ/cm$^2$). The piece DE is going along the melting curve "melt". During supersonic propagation this peace does not change in time. After the end of 2T stage, the pressures D and E continue to conserve while temperature drops down. Conservation of those pressures is connected with separation of the step piece from a temperature distribution and propagation of the piece together with f-characteristics, see Figs. 1 and 3. *Middle panel.* Propagation of compression waves simulated by three codes. Aluminum film is irradiated through glass window,[25] $F_{abs} = 130$ mJ/cm$^2$. *Right panel.* Comp. of pump-probe[25] experimental data with results of simulations done by three codes. We see that addition of elasticity into 2T-HD codes does matter stiffer, therefore a wave runs faster. In MD simulation an aluminum is even more stiffer. We see that experimental results are in between the MD and the 2T-HD+Elast simulations.

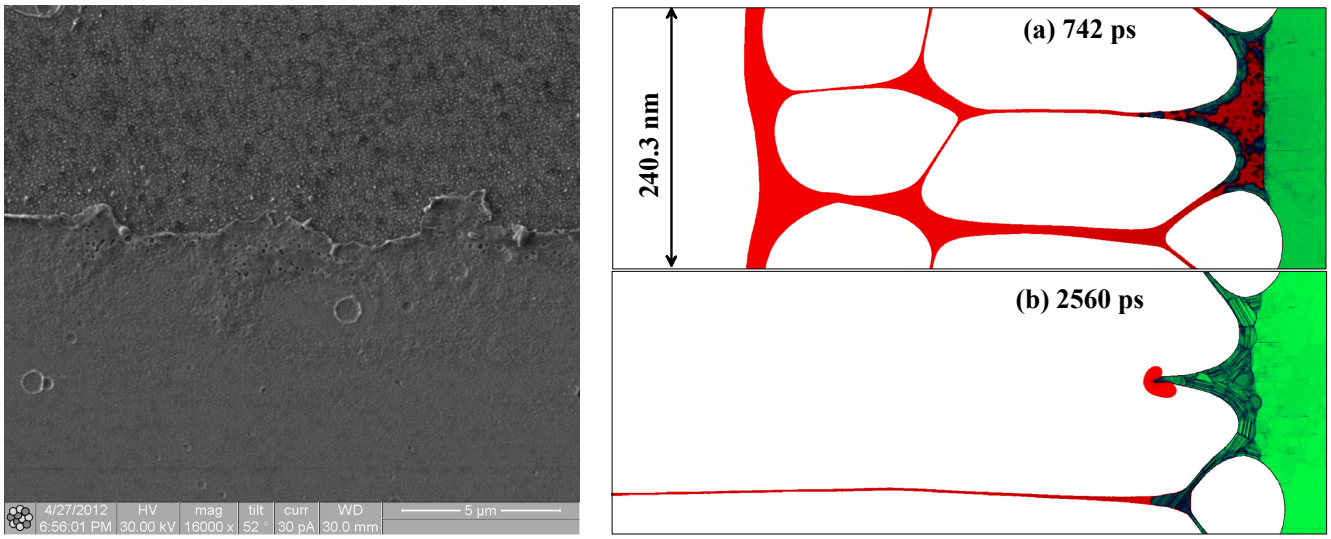


Figure 8. *Left panel.* The edge of crater produced by laser at a tantalum surface. In picture the crater is above the edge. There are small holes in the area near but outside the crater edge. They are signs of ruptured undersurface bubbles.[63] Focused ion beam (FIB) in an imaging mode is used to obtain this picture. There is a low beam current in this mode. In an imaging mode FIB easily achieves 2-5 nm resolution defined by diameter of an ion beam. *Right panel.* Very large scale (172 millions of atoms) long (up to few ns) MD simulation of ablation of Al; $F_{abs}120$ mJ/cm$^2$, $\tau_L = 100$ fs. There are successive stages of nucleation, foaming, strong expansion of foam, and breaking of foam membranes together with freezing of membranes near the internal boundary of foam. Very long (micron scale!) frozen filaments are formed from frozen membranes. Red color correspond to molten Al, green - solid, the dark green areas are formed from nano-crystallites.

are connected with formation and evolution of a two-phase vapor-liquid layer, see Fig. 3. Spallation plate begins to form between nucleation $F_{nucl}$ and ablation $F_{abl}$ thresholds but it can't break away since $F < F_{abl}$. There are ruptured and survived undersurface bubbles[63] near threshold $F_{abl}$. They are seen below the crater edge in Fig. 8 (left). The edge corresponds to the threshold $F_{abl}$. Surface layer (this is a spallation plate) is elevated near the edge. Inside a crater this layer (a spallation plate) flies away, and internal metal layers are opened.

The crater at Ta surface shown in Fig. 8 (left) appears after irradiation by a single p-polarized pulse of powerful Cr:Forsterite laser ($\tau_L = 100$ fs, $\lambda = 1.24$ microns). Angle of incidence was 45 degrees. Tantalum film approximately one micron thick was deposited onto a glass substrate. Film was irradiated from a vacuum side (we call it a frontal boundary), glass substrate is below a frontal surface. Absorbed fluence was $F_{abs} = 180$ mJ/cm$^2$ at a center of a focal spot. The central fluence slightly exceeds (about 20%) ablation threshold.

Undersurface structure of a target (Ta film on substrate) in the peripheral area of the ablation crater (this area is shown in Fig. 8 left) has been studied using focused ion beam (FIB) technique for high-precision milling. This approach on Ta is similar to the approach used in the case of Al analyzed in paper.[63] The study shows that in the case of Ta undersurface bubbles also exist.

Powerful multiprocessors computers and state-of-art massive[64–66] parallel code MPD$^3$ have been used to study late stage (few ns) when decay and freezing of foam begins. Molten metal at this stage is strongly overcooled. Therefore propagation velocity of a recrystallization front is diffusion-limited. Volume crystallization begins as a result of strong overcooling. Crystallin nuclei are seen as the green spots inside a red melt in Fig. 8 (right). Nuclei also germinate at a free surface of melt. After rupture of a membrane forming walls of a bubble, the droplets at the ends of membranes begin to move in direction to a target. This motion stops after full freezing of the membrane and the droplet. The motion is caused by stretching of membrane before its rupture. Even at very late instant shown in Fig. 8 (right), the droplet remains unfrozen. There are frozen bubbles and jets at the tops of those bubbles similar to nanojets observed in experiments of Chichkov et al.[67,68] and Nakato et al.[69]

## ACKNOWLEDGMENTS

The work of M.B.A., S.I.Ash., V.V.Zh., N.A.I., K.P.M., Yu.V.P., and V.A.Kh. was supported by the Russian Foundation for Basic Research (project no. 13-08-01095). MD simulations were performed using the NSF XSEDE facilities and the USF Research Computing Cluster.

## REFERENCES

[1] Anisimov, S., Kapeliovich, B., and Perel'man, T., "Electron emission from metal surfaces exposed to ultrashort laser pulses," *Sov. Phys. JETP* **39**, 375–377 (1974).

[2] Inogamov, N. A., Petrov, Y. V., Anisimov, S. I., Oparin, A. M., Shaposhnikov, N. V., von der Linde, D., and Meyer-ter Vehn, J., "Expansion of matter heated by an ultrash. laser pulse," *JETP Lett.* **69**, 310 (1999).

[3] Inogamov, N., Petrov, Y., Zhakhovsky, V., Khokhlov, V., Demaske, B., Ashitkov, S., Khishchenko, K., Migdal, K., Agranat, M., .Anisimov, S., and Fortov, V., "Two-temperature thermodynamic and kinetic proporties of transition metals irradiated by fs lasers," *AIP Conf. Proc.* **1464**, 593–608 (2012).

[4] Anisimov, S., Zhakhovskii, V., Inogamov, N., Nishihara, K., Petrov, Y., and Khokhlov, V. A., "Ablated matter expansion and crater form. under the action of ultrash. laser pulse," *JETP* **103**, 183–197 (2006).

[5] Inogamov, N. A. and Petrov, Y. V., "Thermal conductivity of metals with hot electrons," *JETP* **110**(3), 446–468 (2010).

[6] Petrov, Y. V., Inogamov, N. A., and Migdal, K. P., "Thermal conductivity and the electron-ion heat transfer coefficient in condensed media with a strongly excited electron subsystem," *JETP Lett.* **97**, 20–27 (2013).

[7] Petrov, Y. V. and Inogamov, N. A., "Removal of mott's interband s-d amplif. of electrical resistance of ni and pt as result of excitation of electrons by fs laser pulse," *Pisma ZhTEF* **98**, 316–322 (2013).

[8] Petrov, Y. V., "Energy exchange between the lattice and electrons in a metal under femtosecond laser irradiation," *Laser and Particle Beams* **23**, 283–289 (2005).

[9] Inogamov, N., Anisimov, S., Zhakhovsky, V., Faenov, A., Petrov, Y., Khokhlov, V., Fortov, V., Agranat, M., Ashitkov, S., Komarov, P., Skobelev, I., Kato, Y., Pikuz, T., Shepelev, V., Fukuda, Y., Tanaka, M., Kishimoto, M., Ishino, M., Nishikino, M., Kando, M., Kawachi, T., Nagasono, M., Ohashi, H., Yabashi, M., Tono, K., Senda, Y., Togashi, T., and Ishikawa, T., "Ablation by short optical and x-ray laser pulses," *SPIE Proceedings* **7996**, 79960T (2011).

[10] Inogamov, N., Faenov, A., Zhakhovsky, V., Pikuz, T., Skobelev, I., Petrov, Y., Khokhlov, V., Shepelev, V., Anisimov, S., Fortov, V., Fukuda, Y., Kando, M., Kawachi, T., Nagasono, M., Ohashi, H., Yabashi, M., Tono, K., Senda, Y., Togashi, T., and Ishikawa, T., "Two-temperature warm dense matter produced by ultrashort extreme vacuum ultraviolet- free electron laser (euv-fel) pulse," *Contributions to Plasma Physics* **51**(5), 419–426 (2011).

[11] Lin, Z., Zhigilei, L. V., and Celli, V., "Electron-phonon coupling and electron heat capacity of metals under conditions of strong electron-phonon nonequilibrium," *Phys. Rev. B* **77**, 075133 (2008).

[12] Rethfeld, B., Kaiser, A., Vicanek, M., and Simon, G. *Phys. Rev. B* **65**, 214303 (2002).

[13] Amoruso, S., Bruzzese, R., Wang, X., and Atanasov, P., "Femtosecond laser ablation of nickel in vacuum," *J. Phys. D.: Appl. Phys.* **40**, 331–340 (2007).

[14] Kanavin, A., Smetanin, I., Isakov, V., Afanasiev, Y., Chichkov, B., Wellegehausen, B., Nolte, S., Momma, C., and Tunnermann, A., "Heat transport in metals irradiated by ultrashort laser pulses," *Phys. Rev. B* **57**, 14698–14703 (1998).

[15] Loboda, P., Smirnov, N., Shadrin, A., and Karlykhanov, N., "Simulation of absorption of femtosecond laser pulses in solid-density copper," *High Energy Density Physics* **7**, 361 (2011).

[16] Agranat, M. B., Anisimov, S. I., Ashitkov, S. I., Zhakhovskii, V. V., Inogamov, N. A., Nishihara, K., Petrov, Y. V., Fortov, V. E., and Khokhlov, V. A., "Dynamics of plume and crater formation after action of femtosecond laser pulse," *Appl. Surf. Sci.* **253**, 6276–6282 (2007).

[17] Agranat, M. B., Anisimov, S. I., Ashitkov, S. I., Zhakhovskii, V. V., Inogamov, N. A., Nishihara, K., and Petrov, Y. V., "Nanospallation induced by a femtosecond laser pulse," *Proc. SPIE 6720* .

[18] Inogamov, N. A., Zhakhovskii, V. V., Ashitkov, S. I., Petrov, Y. V., Agranat, M. B., Anisimov, S. I., Nishihara, K., and Fortov, V. E., "Nanospall. induced by an ultrash. laser pulse," *JETP* **107**, 1–19 (2008).

[19] Inogamov, N. A., Anisimov, S. I., Petrov, Y. V., Khokhlov, V. A., Zhakhovskii, V. V., Nishihara, K., Agranat, M. B., Ashitkov, S. I., and Komarov, P. S., "Theoretical and experimental study of hydrodynamics of metal target irradiated by ultrashort laser pulse," in [*Proc. of SPIE. High-Power Laser Ablation VII*],

[20] Petrov, Y. V., Zhakhovskii, V. V., Inogamov, N. A., Ashitkov, S. I., Khokhlov, V. A., Upadhyay, A. K., Agranat, M. B., Anisimov, S. I., Nishihara, K., Rethfeld, B., and Urbassek, H. M., "Equation of state of matter irradiated by short laser pulse and geometry of spalled cupola," *Proc. of SPIE* .

[21] Anisimov, S., Inogamov, N., Petrov, Y., Khokhlov, V., Zhakhovskii, V., Nishihara, K., Agranat, M., Ashitkov, S., and Komarov, P., "Thresholds for frontal ablation and backside spallation of thin foil irradiated by femtosecond laser pulse," *Appl. Phys. A* **92**(4), 797–801 (2008).

[22] Zhigilei, L. V., Lin, Z., and Ivanov, D. S., "Atomistic modeling of short pulse laser ablation of metals: Connections between melting, spallation, and phase explosion," *J. Phys. Chem. C* **113**(27), 11892 (2009).

[23] Zhakhovskii, V., Inogamov, N., Petrov, Y., Ashitkov, S., and Nishihara, K., "Md simulation of femtosecond ablation and spallation with different interatomic potentials," *Appl. Surf. Sci.* **255**, 9592 (2009).

[24] Karim, E. T., Lin, Z., and Zhigilei, L. V., "Molecular dynamics study of femtosecond laser interactions with cr targets," *AIP Conf. Proc.* **1464**, 280–293 (2012).

[25] Agranat, M., Anisimov, S., Ashitkov, S., Zhakhovskii, V., Inogamov, N., Komarov, P., Ovchinnikov, A., Fortov, V., Khokhlov, V., and Shepelev, V., "Strength properties of an aluminum melt at extremely high tension rates under the action of femtosecond laser pulses," *JETP Lett.* **91**, 471–477 (2010).

[26] Ashitkov, S., Agranat, M., Kanel', G., Komarov, P., and Fortov, V., "Behavior of aluminum near an ultimate theoretical strength in experiments with femtosecond laser pulses," *JETP Lett.* **92**, 516–520 (2010).

[27] Ashitkov, S., Inogamov, N., Komarov, P., Zhakhovsky, V., Oleynik, I., Agranat, M., Kanel, G., and Fortov, V., "Strength of metals in liquid and solid states at extremely high tension produced by femtosecond laser heating.," *AIP Conference Proceedings* **1464**, 120–125 (2012).

[28] Inogamov, N., Faenov, A., Khokhlov, V., Zhakhovskii, V., Petrov, Y., Skobelev, I., Nishihara, K., Kato, Y., Tanaka, M., Pikuz, T., Kishimoto, M., Ishino, M., Nishikino, M., Fukuda, Y., Bulanov, S., Kawachi, T., Anisimov, S., and Fortov, V., "Spallative ablation of metals and dielectrics," *Contributions to Plasma Physics* **49**(7-8), 455–466 (2009).
[29] Demaske, B., Zhakhovsky, V., Inogamov, N., and Oleynik, I., "Ablation and spallation of gold films irradiated by ultrashort laser pulses," *Phys. Rev. B* **82**, 064113 (2010).
[30] Zhakhovsky, V., Demaske, B., Inogamov, N., Khokhlov, V., Ashitkov, S., Agranat, M., and Oleynik, I., "Super-elastic response of metals to laser-induced shock waves," *AIP Conf. Proc.* **1464**, 102–112 (2012).
[31] Demaske, B., Zhakhovsky, V., Inogamov, N., and Oleynik, I., "Molecular dynamics simulations of femtosecond laser ablation and spallation of gold," in [*Intern. Symp. High Power Laser Ablation, Eldorado Hotel, Santa Fe, NM, 19-22 APRIL 2010, Proc.*], *AIP Conference Proceedings* **1278**, 121–130 (2010).
[32] Demaske, B., Zhakhovsky, V., Inogamov, N., White, C., and Oleynik, I., "Md simulations of laser-induced ultrashort shock waves in nickel," *AIP Conference Proceedings* **1426**, 1163–1166 (2012).
[33] Demaske, B. J., Zhakhovsky, V. V., Inogamov, N. A., and Oleynik, I. I., "Ultrashort shock waves in nickel induced by femtosecond laser pulses," *Phys. Rev. B* **87**(5), 054109 1–9 (2013).
[34] Bushman, A. V., Kanel', G. I., Ni, A. L., and Fortov, V. E., [*Intense dynamic loading of condensed matter*], Taylor & Francis (1993).
[35] Kanel, G. I., Razorenov, S. V., and Fortov, V. E., [*Shock-Wave Phenomena and the Properties of Condensed Matter*], Springer (2004).
[36] Antoun, T., Seaman, L., Curran, D. R., Kanel, G. I., Razorenov, S. V., and Utkin, A. V., [*Spall Fracture (Shock Wave and High Pressure Phenomena)*], Springer (2003).
[37] Kanel, G. I., Fortov, V. E., and Razorenov, S. V., "Shock waves in condensed-state physics," *Phys. Usp.* **50**, 771 (2007).
[38] Misochko, O. V., "Non-classical excited states of crystal lattice: squeezed and entagled phonons," *Uspekhi Fizicheskikh Nauk* **183**(9), 917–933 (2013).
[39] Zijlstra, E. S., Kalitsov, A., Zier, T., and Garcia, M. E., "Squeezed thermal phonons precurse nonthermal melting of silicon as a function of fluence," *Phys. Rev. X* **3**, 011005 (2013).
[40] Gamaly, E. G. and Rode, A. V., "Ultrafast electronic relaxation in superheated bismuth," *New J. Phys.* **15**, 013035 (2013).
[41] Khakshouri, S., Alfe, D., and Duffy, D. M., "Development of an electron-temperature-dependent interatomic potential for molecular dynamics simulation of tungsten under electronic excitation," *Phys. Rev. B* **78**, 224304 (2008).
[42] Sin'ko, G. V., Smirnov, N. A., Ovechkin, A. A., Levashov, P. R., and Khishchenko, K. V., "Thermodynamic functions of the heated electron subsystem in the field of cold nuclei," *High Energy Density Physics* **9**, 309–314 (2013).
[43] Kresse, G. and Furthmuller, J., "Efficiency of ab initio total energy calculations for metals and semiconductors using a plane-wave basis set," *Computational Materials Science* **6**, 15–50 (1996).
[44] *http://teos.ficp.ac.ru/rusbank/*.
[45] Rose, J. H., Smith, J. R., Guinea, F., and Ferrante, J., "Universal features of the equation of state of metals," *Phys. Rev. B* **29**, 2963 (1984).
[46] Evans, R., Badger, A. D., Fallies, F., Mahdieh, M., Hall, T. A., Audebert, P., Geindre, J.-P., Gauthier, J.-C., Mysyrowicz, A., Grillon, G., and Antonetti, A. *Phys. Rev. Lett.* **77**, 3359–3362 (1996).
[47] Gahagan, K. T., Moore, D. S., Funk, D. J., Rabie, R. L., Buelow, S. J., and W., N. J., "Measurement of shock wave rise times in metal thin films," *Phys. Rev. Lett.* **85**, 3205–3208 (2000).
[48] Funk, D. J., Moore, D. S., Gahagan, K. T., Buelow, S. J., Reho, J. H., Fisher, G. L., and Rabie, R. L., "Ultrafast measurement of the optical properties of aluminum during shock-wave breakout," *Phys. Rev. B* **64**, 115114 (Aug 2001).
[49] Ashitkov, S., Komarov, P., Agranat, M., Kanel, G., and Fortov, V., "Measurements of a strength of metals in a picosecond time range," in [*18th Biennial Intl. Conference of the APS Topical Group on Shock Compression of Condensed Matter held in conjunction with the 24th Biennial Intl. Conference of the Intl. Association for the Advancement of High Pressure Science and Technology (AIRAPT), Seattle*], *Bulletin of the American Physical Society* **58**(7), 187–188, V6 4 (2013).

[50] Whitley, V. H., McGrane, S. D., Eakins, D. E., Bolme, C. A., Moore, D. S., and Bingert, J. F., "The elastic-plastic response of al films to ultrafast laser-generated shocks," *J. Appl. Phys.* **109**, 013505 (2011).

[51] Crowhurst, J. C., Armstrong, M. R., Knight, K. B., Zaug, J. M., and Behymer, E. M., "Invar.of the dissip. action at ultrahigh strain rates above the strong shock threshold," *Phys. Rev. Lett.* **107**, 144302 (2011).

[52] Zhakhovskii, V. V. and Inogamov, N. A., "Elastic-plastic phenomena in ultrashort shock waves," *JETP Lett.* **92**, 521–526 (2010).

[53] Zhakhovsky, V. V., Budzevich, M. M., Inogamov, N. A., Oleynik, I. I., and White, C. T., "Two-zone elastic-plastic single shock waves in solids," *Phys. Rev. Lett.* **107**(13), 135502 (4) (2011).

[54] Inogamov, N., Zhakhovskii, V., Khokhlov, V. A., and Shepelev, V., "Superelasticity and the propagation of shock waves in crystals," *JETP Lett.* **93**(4), 226–232 (2011).

[55] Huang, L., Yang, Y., Wang, Y., Zheng, Z., and Su, W., "Measurement of transit time for femtosecond-laser-driven shock wave through aluminium films by ultrafast microscopy," *J. Phys. D.* **42**, 045502 (2009).

[56] Demaske, B., Zhakhovsky, V., Inogamov, N., White, C., and Oleynik, I., "Split and two-zone elastic-plastic shock waves in nickel: a md study," in [*18th Biennial Intl. Conf. APS Topical Group on Shock Compr. Cond.Matter held in conjunction with the 24th Biennial Intl. Conf. Intl. Association Advancement High Pressure Sci. and Tech. (AIRAPT), Seattle*], *Bulletin Amer. Phys. Soc.* **58**(7), 151–152, Q6 5 (2013).

[57] Inogamov, N., Ashitkov, S., Zhakhovsky, V., Shepelev, V., Khokhlov, V., Komarov, P., Agranat, M., Anisimov, S., and Fortov, V., "Acoustic probing of two-temperature relaxation initiated by action of ultrashort laser pulse," *Appl. Phys. A* **101**, 1–5 (2010).

[58] Inogamov, N., Zhakhovsky, V., Ashitkov, S., Khokhlov, V., Shepelev, V., Komarov, P., Ovchinnikov, A., Sitnikov, D., Petrov, Y., Agranat, M., Anisimov, S., and Fortov, V., "Laser acoustic probing of two-temperature zone created by femtosecond pulse," *Contributions to Plasma Physics* **51**(4), 367–374 (2011).

[59] Inogamov, N. A., Zhakhovskii, V. V., Ashitkov, S. I., Khokhlov, V. A., Petrov, Y. V., Komarov, P. S., Agranat, M. B., Anisimov, S. I., and Nishihara, K., "Two-temperature relaxation and melting after absorption of femtosecond laser pulse," *Applied Surface Science* **255**, 9712–9716 (2009).

[60] Starikov, S., Stegailov, V., Norman, G., Fortov, V., Ishino, M., Tanaka, M., Hasegawa, N., Nishikino, M., Ohba, T., Kaihori, T., Ochi, E., Imazono, T., Kavachi, T., Tamotsu, S., Pikuz, T., Skobelev, I., and Faenov, A., "Laser ablation of gold: experiment and atomistic simlation," *JETP Lett.* **93**(11), 642–647 (2011).

[61] Norman, G., Starikov, S., and Stegailov, V., "Atomistic simlation of laser ablation of gold: effect of pressure relaxation," *JETP* **114**(5), 792–800 (2012).

[62] Norman, G. E., Starikov, S. V., Stegailov, V. V., Saitov, I. M., and Zhilyaev, P. A., "Atomistic modeling of warm dense matter in the two-temperature state," *Contrib. Plasma Phys.* **53**, 129–139 (2013).

[63] Ashitkov, S., Inogamov, N., Zhakhovsky, V., Emirov, Y., Agranat, M., Oleinik, I., Anisimov, S., and Fortov, V., "Formation of nanocav. in surface layer of al target irrad. by fs laser pulse," *JETP Lett.* **95**, 176 (2012).

[64] arXiv:DC/0405086v1 24 May 2004.

[65] Zhakhovskii, V. V., Inogamov, N. A., and Nishihara, K., "Laser ablation and spallation of crystalline aluminum simulated by molecular dynamics," *J. Phys.: Conf. Ser.* **112**, 042080 (2008).

[66] Zhakhovskii, V. V., Inogamov, N. A., and Nishihara, K., "New mechanism of the formation of the nanorelief on a surface irradiated by a femtosecond laser pulse," *JETP Lett.* **87**, 423–427 (2008).

[67] Kuznetsov, A., Koch, J., and Chichkov, B., "Nanostructuring of thin gold films by femtosecond lasers," *Appl. Phys. A* **94**, 221–230 (2009).

[68] Ivanov, D., Kuznetsov, A., Lipp, V., Rethfeld, B., Chichkov, B., Garcia, M., and Schulz, W., "Short laser pulse nanostr.of metals: direct comp.of md modeling and experiment," *Appl. Phys. A* **111**, 675687 (2013).

[69] Nakata, Y., Tsuchida, K., Miyanaga, N., and Okada, T., "Nano-sized and periodic structures generated by interfering femtosecond laser," *JLMN-Journal of Laser Micro/Nanoengineering* **3**(2), 63–66 (2008).